Water Resources Research

RESEARCH ARTICLE
10.1029/2023WR035084

Stochastic Dynamics of Two-Dimensional Particle Motion in Darcy-Scale Heterogeneous Porous Media

Aronne Dell'Oca[1] and **Marco Dentz**[2]

[1]Dipartimento di Ingegneria Civile e Ambientale (DICA), Politecnico di Milano, Milan, Italy, [2]Spanish National Research Council (IDAEA-CSIC), Barcelona, Spain

Key Points:

- Flow topology determines transverse particle motion
- Transverse motion follows a correlated Brownian motion
- Stochastic time-domain random walk model captures full two-dimensional particle transport

Correspondence to:

M. Dentz,
marco.dentz@csic.es

Citation:

Dell'Oca, A., & Dentz, M. (2023). Stochastic dynamics of two-dimensional particle motion in Darcy-scale heterogeneous porous media. *Water Resources Research*, *59*, e2023WR035084. https://doi.org/10.1029/2023WR035084

Received 11 APR 2023
Accepted 31 AUG 2023

Author Contributions:

Conceptualization: Aronne Dell'Oca, Marco Dentz
Data curation: Aronne Dell'Oca
Formal analysis: Aronne Dell'Oca
Funding acquisition: Aronne Dell'Oca, Marco Dentz
Investigation: Aronne Dell'Oca
Methodology: Aronne Dell'Oca, Marco Dentz
Project Administration: Aronne Dell'Oca, Marco Dentz
Software: Aronne Dell'Oca
Supervision: Marco Dentz
Validation: Aronne Dell'Oca, Marco Dentz
Visualization: Aronne Dell'Oca
Writing – original draft: Aronne Dell'Oca, Marco Dentz

Abstract We study the upscaling and prediction of ensemble dispersion in two-dimensional heterogeneous porous media with focus on transverse dispersion. To this end, we study the stochastic dynamics of the motion of advective particles that move along the streamlines of the heterogeneous flow field. While longitudinal dispersion may evolve super-linearly with time, transverse dispersion is characterized by ultraslow diffusion, that is, the transverse displacement variance grows asymptotically with the logarithm of time. This remarkable behavior is linked to the solenoidal character of the flow field, which needs to be accounted for in stochastic models for the two-dimensional particle motion. Here, we derive an upscaled model based on the statistical characterization of the motion of solute particles. To this end, we analyze particle velocities and orientations through equidistant sampling along the particle trajectories obtained from direct numerical simulations. This sampling strategy respects the flow structure, which is organized on a characteristic length scale. Perturbation theory shows that the longitudinal particle motion is determined by the variability of travel times, while the transverse motion is governed by the fluctuations of the space increments. The latter turns out to be strongly anticorrelated with a correlation structure that leads to ultraslow diffusion. Based on this analysis, we derive a stochastic model that combines a correlated Gaussian noise for the transverse motion with a spatial Markov model for the particle speeds. The model results are contrasted with detailed numerical simulations in two-dimensional heterogeneous porous media of different heterogeneity variances.

Plain Language Summary The hydraulic conductivity of environmental geological formation can exhibit strong spatial variations. This leads to the formation of complex flow fields, where the flow tends to by-pass low conductivity areas and focuses within preferential flow paths. This complexity controls the transport dynamics of dissolved chemicals. Moreover, due to the lack of knowledge about the details of the formation and its properties, we employ a stochastic approach to predict the fate of transported solutes. We propose a stochastic model for large-scale solute transport in two-dimensional heterogeneous Darcy flow in which we incorporate key physical transport mechanisms that occur in the direction aligned with and transverse to the mean direction of flow.

1. Introduction

Non-Fickian solute transport can manifest in the nonlinear scaling of dispersion, non-Gaussian concentration distributions, and early and late solute arrivals. Such behaviors have been documented in heterogeneous porous and fractured media from the pore to the regional scales (Adams & Gelhar, 1992; Berkowitz et al., 2006; Bijeljic et al., 2011; De Smedt & Wierenga, 1984; Neuman & Tartakovsky, 2009; Silliman & Simpson, 1987). The quantitative understanding of these behaviors plays a central role for the prediction of large-scale solute transport in environmental and industrial applications ranging from groundwater management and remediation (Domenico & Schwartz, 1998) to geological carbon dioxide storage (Niemi et al., 2017).

In the present work, we focus on the transport of solute in two-dimensional Darcy-scale porous media that are characterized by spatial variability in the hydraulic conductivity. On the local scale, that is, on length scales smaller that the characteristic length scale of heterogeneity, solute dispersion is dominated by diffusion and mechanical dispersion caused by velocity variations on the pore scale. At scales larger than the characteristic heterogeneity length scale, dispersion is dominated by the heterogeneity of the hydraulic conductivity field and flow velocity. Large-scale applications dealing with solute transport in geological media are concerned with scales on the order of 10–100 times the characteristic correlation length of the hydraulic conductivity, at which the advective component of the motion is the prevailing factor controlling the dispersive behavior of solutes

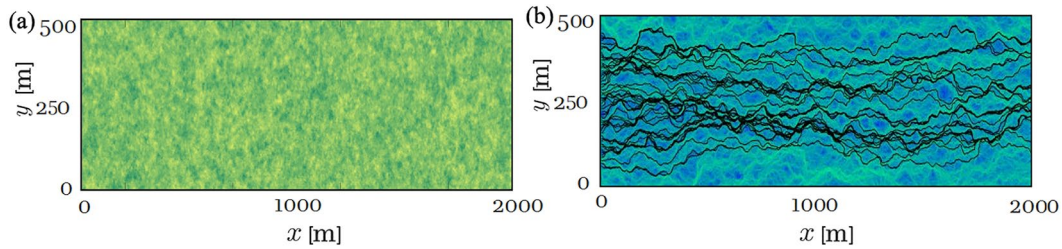

Figure 1. Left panel: Spatial distribution of the logarithm of the hydraulic conductivity $Y(\mathbf{x})$ and Right panel: spatial organization of the module of the Darcy' velocity (logarithmic scale, blue low, and green high) considering a strongly heterogeneous geological formation. Samples of particle trajectories are also drawn (black curves): note the emergence of preferential flow paths characterized by meandering-like structures as we proceed downstream from the injection location. The variance of $Y(\mathbf{x})$ is $\sigma_Y^2 = 4$, its correlation length is 10 m.

(Rubin, 2003). Thus, we focus on purely advective transport. We consider two-dimensional Darcy flows, which can represent flow in shallow aquifers, three-dimensional formations characterized by a large correlation length in one spatial direction (e.g., stratification) (Rubin, 2003), as well as flow in rough fractures (Hu et al., 2020; Kong & Chen, 2018; Kottwitz et al., 2020; Z. Wang et al., 2020; Zimmerman & Bodvarsson, 1996).

The hidden nature of the structure of geological formations, in combination with spatial variations in their hydraulic properties, has led to the development of stochastic models to predict the fate of dissolved substances (Berkowitz et al., 2006; Dell'Oca et al., 2018, 2019; Frippiat & Holeyman, 2008; Neuman & Tartakovsky, 2009; Rubin, 2003). In this context, major efforts have been devoted to conceptualize and formalize stochastic models to quantify average solute transport along the mean flow direction. These efforts include stochastic perturbation theory (Rubin, 2003), self-consistent time-domain random walk (TDRW) formulations (Cvetkovic et al., 2014; Fiori et al., 2013, 2015) through the use of fractional advection-diffusion equations (Benson et al., 2000; Y. Zhang et al., 2009), multirate mass transfer approaches (Haggerty & Gorelick, 1995; Harvey & Gorelick, 2000), and continuous time random walks (Comolli et al., 2019; Dentz et al., 2020; Edery et al., 2014).

Transverse dispersion can be measured by the displacement variance of solute particles (Dagan, 1989). Using stochastic perturbation theory, it has been shown (Dagan, 1984) that transverse ensemble dispersion grows ballistically at short times, that is with the square of time, and eventually crosses over to an ultraslow dispersive behavior that is characterized by a growth with the logarithm of time. As a consequence, the transverse dispersion coefficient, which is defined in terms of the time-derivative of the displacement variance, decays asymptotically to zero in the absence of local dispersion. This is an exact result, which can be derived without recourse to perturbation theory (Attinger et al., 2004), and which has been observed in direct numerical simulations of flow and transport in two-dimensional heterogeneous porous media (Bellin et al., 1992; de Dreuzy et al., 2007; Salandin & Fiorotto, 1998). This ultraslow dispersion behavior is intimately linked to the meandering of the streamlines that arise because the flow field is divergence-free. The streamline meandering is illustrated in Figure 1, which shows a colormap of the flow speeds together with a set of purely advective particle trajectories. It is interesting to note that ultraslow dispersion emerges in a variety of systems characterized by crowded or confined environments such as dense colloids (Boettcher & Sibani, 2011) and colloidal hard-sphere system (Sperl, 2005), for vacancy-mediated diffusive motion (Bénichou & Oshanin, 2002), and diffusion in a random force landscapes (Havlin & Ben-Avraham, 2002), but also in human mobility (Song et al., 2010). In the context of flow in two-dimensional porous media, the confinement arises from the fact that the flow is divergence-free, which dictates the spatial organization of the streamlines.

The constraint imposed by the flow topology on transverse dispersion needs to be reflected in large-scale transport models for streamwise and transverse solute dispersion. The multi-dimensional CTRW approach of Dentz et al. (2004) represents transverse dispersion in heterogeneous media through uncorrelated Gaussian-distributed space increments combined with random transition times. W. Wang and Barkai (2020) derive a two-dimensional fractional-in-space advection-dispersion equation based on this approach to represent the bulk dispersion behavior in geological media. These models do not account for the topological constraints imposed by the divergence-free Darcy flow equation. In fact, this type of CTRW represents particle motion under spatially random retardation properties (Dentz & Castro, 2009).

Meerschaert et al. (2001) proposed a multi-dimensional fractional diffusion model to capture super-diffusive anisotropic transport regimes along the longitudinal and the transverse directions. Y. Zhang and Benson (2013)

use a two-dimensional space-time fractional approach with space-dependent diffusion coefficients to model the vertically integrated tritium plumes of the MADE-2 experiment. Also, these frameworks do not account for the impact of topological constraints on transverse dispersion.

Meyer and Tchelepi (2010) propose a Langevin model for the Markovian time evolution of streamwise and transverse particle velocities (Markovian velocity process, MVP) that uses drift and diffusion coefficients that are obtained by calibrating suitable continuous functions to Monte Carlo simulations of the direct flow and transport problem. This formulation satisfactorily reproduces the evolution of longitudinal and transverse dispersion. Meyer et al. (2013) modify the framework by focusing on the Markovian character in time of the streamwise velocities and the solute particle orientation angle (Polar MVP, PMVP). The latter formulation results in model predictions of higher quality with respect to the MVP formulation.

Notably, Meyer (2018) and Meyer et al. (2013) highlight the time independence between the streamwise velocity and the orientation, which greatly simplifies the formulation of the PMVP and, more generally, of two-dimensional stochastic transport models.

Furthermore, Dünser and Meyer (2016) applied the PMVP to the non-stationary field macrodispersion experiment (MADE) obtaining a good overall agreement with reference to Monte Carlo results. In addition, considering low degrees of heterogeneity, Meyer (2017) simplifies the parametrization of the MVP model by leveraging on perturbation theory results. In a similar fashion, Meyer (2018) considers higher degrees of heterogeneity and relates the PMVP parameters to perturbation theory, while accounting for the deviation from Gaussianity in the distribution of the streamwise velocity.

As discussed above, currently non-Fickian transport approaches such as CTRW and FADE are not able to account for the impact of topological constraints on transverse dispersion. The main scientific question is how to represent (non-Fickian) longitudinal and transverse particle motion in an effective stochastic modeling framework that respects topological constraints. To this end, we study particle speeds and orientations sampled equidistantly along trajectories from detailed numerical flow and transport simulations. Based on this analysis and using exact analytical expressions for the autocorrelation function of the orientation angle, we propose a stochastic approach for the two-dimensional particle motion that explicitly accounts for the constraint imposed on transverse particle motion by the flow topology. Our formulation relates to that of Meyer (2018) and Meyer et al. (2013) since equidistantly sampled particle speeds and orientations can be treated as independent stochastic processes, where the former exhibits Markovianity. On the other hand, the equidistantly sampled particle orientation is characterized by a persistent degree of anticorrelation, which we take into account explicitly in the definition of our stochastic model.

Section 2 poses the flow and transport problem in two-dimensional heterogeneous porous media, defines the target variables and describes the direct numerical simulations. Section 3 reports on the quantification of the stochastic particle motion using perturbation theory for weak heterogeneity and in terms of a stochastic TDRW model for strong heterogeneity of the medium. Section 4 validates the derived two-dimensional model against detailed numerical simulations.

2. Flow and Transport in Heterogeneous Porous Media

In this section, we provide the details about the heterogeneous spatial arrangement of the hydraulic conductivity field, and the Darcy scale flow and transport problem. Furthermore, we define the transport-related observables.

2.1. Darcy Flow and Hydraulic Conductivity

Flow in porous media is described on the continuum scale by the Darcy equation (Bear, 1972)

$$\mathbf{q}(\mathbf{x}) = -K(\mathbf{x})\nabla h(\mathbf{x}), \tag{1}$$

where $\mathbf{x}$ denotes the two-dimensional space coordinate vector with components x and y, $\mathbf{q}$ is the Darcy flux vector (with components q_x and q_y) and $h(\mathbf{x})$ is the hydraulic head. We restrict the analysis to the case in which the hydraulic conductivity $K(\mathbf{x})$ is a scalar. We do not consider sinks or sources and consider fluid and solid matrix as incompressible such that $\nabla \cdot \mathbf{q} = 0$.

In order to quantify the spatial variability of the hydraulic conductivity, we model $K(\mathbf{x})$ as a multi-Gaussian random field with a lognormal marginal distribution (Rubin, 2003) and geometric mean K_G. That is, the log-hydraulic conductivity $Y(\mathbf{x}) = \ln[K(\mathbf{x})/K_G]$ is represented as a second-order stationary multi-Gaussian random field characterized by zero mean and the isotropic exponential covariance function

$$\langle Y(\mathbf{x})Y(\mathbf{x}')\rangle = \sigma_Y^2 \exp\left(-|\mathbf{x}-\mathbf{x}'|/\ell_Y\right), \tag{2}$$

where, σ_Y^2 and ℓ_Y are the variance and the correlation length of Y, respectively. The angular brackets denote the ensemble average. In the following, all lengths are non-dimensionalized with ℓ_Y. Note that the multi-Gaussian assumption for representing the variability of hydraulic conductivity in geological media has been challenged in the literature (Gómez-Hernández & Wen, 1998; Molz et al., 2004; Painter, 1996; Riva et al., 2015). Here, we choose the representation of $K(\mathbf{x})$ as a multi-Gaussian random field as a generic representation of spatial variability. As transverse dispersion is dominated by the flow field topology, the general conclusions can be transferred also to non-multi-Gaussian random fields.

The mean hydraulic gradient is aligned with the x-direction of the coordinate system such that the mean Darcy velocity is $\langle q_i(\mathbf{x})\rangle = \delta_{i1}\langle q\rangle$, where $\langle q\rangle$ denotes the mean Darcy velocity. The Eulerian fluid velocity vector $\mathbf{v}(\mathbf{x})$ is obtained by rescaling the flux vector as $\mathbf{v}(\mathbf{x}) = \mathbf{q}(\mathbf{x})/\phi$, where ϕ is porosity. In the following, we assume that porosity is constant and set it equal to one, which is equivalent to rescaling time. The Eulerian mean velocity is $\langle v_i(\mathbf{x})\rangle = \delta_{i1}\langle v\rangle$, where $\langle v\rangle$ denotes the mean Eulerian velocity. The characteristic advection time is defined by $\tau_v = \ell_Y/\langle v\rangle$.

The magnitude $v(\mathbf{x}) = |\mathbf{v}(\mathbf{x})|$ of the Eulerian velocity denotes the flow speed. The Eulerian flow field is characterized by the distribution $p_e(v)$. It is obtained by spatial sampling as

$$p_e(v) = \lim_{V\to\infty} \frac{1}{V}\int_\Omega d\mathbf{x}\delta[v - v_e(\mathbf{x})], \tag{3}$$

where Ω is the sampling domain and V is its volume. Due to ergodicity, spatial sampling of v_e is equivalent to ensemble sampling, and thus, $p_e(v) = \langle\delta[v - v_e(\mathbf{x})]\rangle$.

2.2. Particle Motion

We focus on purely advective transport. Thus, we adopt a Lagrangian perspective by considering solute particles of equal mass whose trajectories $\mathbf{x}(t)$ are given by

$$\frac{d\mathbf{x}(t)}{dt} = \mathbf{w}(t), \tag{4}$$

where $\mathbf{w}(t) = \mathbf{v}[\mathbf{x}(t)]$ is the isochronic Lagrangian speed and t is time. The initial particle position is denoted by $\mathbf{x}(t=0) = \mathbf{x}_0$.

The particle speed is given by $w(t) = |\mathbf{w}(t)|$. The point PDF $p_t(v)$ of $w(t)$ sampled over all streamlines is equal to the PDF $p_e(v)$ of Eulerian speeds (Hakoun et al., 2019).

$$p_t(v) = p_e(v). \tag{5}$$

This is a result of the fact that the flow is volume conserving. In the following, we consider a uniform initial distribution of particle positions across the cross-section of the medium. This implies that the distribution $p_0(v)$ of initial speeds $v_0 = w_0(t=0) = v(\mathbf{x}_0)$ is $p_0(v) = p_e(v)$ is equal to $p_e(v)$. That is, the initial speeds distribution is equal to the steady state distribution.

For our analysis, it is convenient to consider the advective particle motion as a function of the streamwise distance (Comolli et al., 2019)

$$\frac{d\hat{\mathbf{x}}(s)}{ds} = \frac{\mathbf{u}(s)}{u(s)}, \quad \frac{dt(s)}{ds} = \frac{1}{u(s)}, \tag{6}$$

where s is the particle streamwise coordinate, $\mathbf{u}(s) = \mathbf{v}\left[\hat{\mathbf{x}}(s)\right]$ is the s-Lagrangian velocity and $u(s) = |\mathbf{u}(s)|$ is the s-Lagrangian speed. The point PDF $p_s(v)$ of $v_s(s)$ is equal to the flux-weighted Eulerian speed PDF (Hakoun et al., 2019).

$$p_s(v) = \frac{v p_e(v)}{\langle v_e \rangle}. \tag{7}$$

The distribution of initial speeds $v_s(s = 0) = v_0 = v_t(t = 0)$ is $p_e(v)$. This implies that the speed statistics evolve toward the steady state $p_s(v)$ with distance along the streamlines. The particle displacement in time is obtained in terms of $\hat{\mathbf{x}}(s)$ as $\mathbf{x}(t) = \hat{\mathbf{x}}[s(t)]$, where $s(t) = \max[s|t(s) \le t]$.

Our goal is to upscale the motion of solute particles that are advected in a stationary Darcy scale heterogeneous flow field. Thus, we consider particle displacements relative to the injection position $\mathbf{x}_0$, that is, $\mathbf{x}'(t) = \mathbf{x}(t) - \mathbf{x}_0$. As descriptors of the stochastic motion of the solute particles, we consider the evolution of the dispersion scales along the longitudinal and the transverse directions, that is,

$$\sigma_x(t) = \sqrt{\left\langle \left[x'(t) - \langle x'(t) \rangle\right]^2 \right\rangle}, \quad \sigma_y(t) = \sqrt{\left\langle \left[y'(t) - \langle y'(t) \rangle\right]^2 \right\rangle}. \tag{8}$$

Along the transverse direction, the average particle position is zero, that is, $\langle y'(t) \rangle = 0$, because the mean flow is aligned with the x-direction of the coordinate system, and $y'(t)$ measures the transverse displacement relative to the injection position. Note that here we define the displacement moments as averages over all particles across all realizations, that is, as ensemble quantities. They measure the longitudinal and transverse spreading across medium realizations (Kitanidis, 1988). Fiori and Janković (2005) discuss under which conditions ensemble moments can be used to estimate dispersion in single aquifer realizations.

The knowledge of the dispersion scales σ_x and σ_y can be insufficient to properly characterize solute transport if the probability distributions of $x'(t)$ and $y'(t)$ are not Gaussian. Thus, we consider also the probability distributions of the longitudinal and transverse particle positions centered to their respective mean, that is,

$$p(x,t) = \langle \delta\left(x - \left[x'(t) - \langle x'(t) \rangle\right]\right) \rangle, \quad p(y,t) = \langle \delta\left[y - y'(t)\right] \rangle. \tag{9}$$

Note that x and y denote the sample-space variables while $x'(t)$ and $y'(t)$ denote random variables. Finally, we also consider the joint probability density function for the longitudinal and transverse particle positions, that is,

$$p(\mathbf{x},t) = \langle \delta\left[\mathbf{x} - \mathbf{x}'(t)\right] \rangle. \tag{10}$$

For simplicity of notation, we omit the primes in the following, and understand that all particle positions are relative to their initial position $\mathbf{x}_0$.

2.3. Numerical Simulations

We consider a two-dimensional domain of size $600\ell_Y \times 150\ell_Y$. Different realizations of $Y(\mathbf{x})$ are generated using a sequential Gaussian simulator (Deutsch & Journel, 1992) on a regular Cartesian grid with element size equal to $\ell_Y/10$. We generate 100 Monte Carlo realizations of $Y(\mathbf{x})$ for three different scenarios with $\sigma_Y^2 = 1, 2$ and 4. Note that the number of Monte Carlo realizations is sufficient to obtain reliable transport statistics, given the extended initial condition of the transport problem described later in this section.

For the flow problem, we impose permeameter-like boundaries conditions, that is, no-flow along the bottom ($y = 0$) and top ($y = 150\ell_Y$) boundaries, a fixed value of the hydraulic head along the left ($x = 0$) boundary and $q_i = \delta_{ix}\langle q \rangle$ along the right ($x = 600\ell_Y$) boundary. Note that, the imposed boundary conditions lead to a uniform in the mean flow, $\langle q_i \rangle = \delta_{ix}\langle q \rangle$. Thus, we identify x as the longitudinal (or mean flow) direction and y as the transverse direction. We use the same grid structure employed for the generation of $Y(\mathbf{x})$. The flow problem is solved numerically using a mixed-finite element solver (Younes et al., 2010). The flow statistics are sampled over a subregion of $560\ell_Y \times 110\ell_Y$ to avoid boundary effects.

The numerical solution of the transport problem is based on the discretized version of Equation 6,

$$\hat{\mathbf{x}}_{n+1} = \hat{\mathbf{x}}_n + \frac{\mathbf{v}_e(\hat{\mathbf{x}}_n)\Delta s}{|\mathbf{v}_e(\hat{\mathbf{x}}_n)|}, \quad t_{n+1} = t_n + \frac{\Delta s}{|\mathbf{v}_e(\hat{\mathbf{x}}_n)|} \tag{11}$$

where $\hat{\mathbf{x}}_n = \hat{\mathbf{x}}(s_n)$, $t_n = t(s_n)$, $s_n = n\Delta s$ and Δs is the constant spatial increment here set to $\Delta s = \ell_Y/100$. We inject 110 particles uniformly spaced over a straight line perpendicular to the mean flow direction covering $90\ell_Y$. The line is placed at distance of $30\ell_Y$ downstream from the $x = 0$ boundary and at distances of $20\ell_Y$ from the lateral boundaries. We employ Pollock's semi-analytical method for particle tracking (Pollock, 1988).

3. Stochastic Particle Motion

In this section, we study the stochastic dynamics of two-dimensional particle motion in random Darcy' flow fields. In heterogeneous porous media, streamlines are tortuous as illustrated in Figure 1. Therefore, the velocity varies along the streamlines. The series $\{w(t)\}$ of isochronously sampled Lagrangian speeds typically exhibits intermittent behavior, that is, long periods of low speeds alternate with short periods of intensively fluctuating high speeds (Hakoun et al., 2019). This intermittent behavior is due to the fact that flow velocities vary on a characteristic length scale, rather than a time scale. Therefore, the residence time in low velocities is higher than in high velocities. As a consequence, the equidistantly sampled velocity series $\{u(s)\}$ is not intermittent. Thus, we consider here particle motion as a function of streamline distance as expressed by Equation 6, that is, in terms of a TDRW. In this context, we first recall results from second-order perturbation theory in the fluctuations of $\mathbf{v}(\mathbf{x})$ about its mean value, which is valid for low and moderate spatial heterogeneity. Then, we use a stochastic TDRW approach to capture two-dimensional particle motion at higher degree of heterogeneity.

3.1. Perturbation Theory

We expand the equations of motion (Equation 6) up to first order in the fluctuations of the random flow field $\mathbf{v}'(\mathbf{x}) = \mathbf{v}(\mathbf{x}) - \langle \mathbf{v} \rangle$. Thus, we obtain

$$\frac{d\hat{x}(s)}{ds} = 1, \qquad \frac{d\hat{y}(s)}{ds} = \frac{v_y\left[\hat{\mathbf{x}}_0(s)\right]}{\langle v \rangle}, \qquad \frac{dt(s)}{ds} = \frac{1}{\langle v \rangle} - \frac{v_x'\left[\hat{\mathbf{x}}_0(s)\right]}{\langle v^2 \rangle}, \tag{12}$$

where $\hat{\mathbf{x}}_0(s) = (s, 0)^\top$. The superscript $\top$ denotes the transpose. Note that $v_y'(\mathbf{x}) = v_y(\mathbf{x})$. We consistently omit terms of quadratic order in the velocity fluctuations. From Equation 12, we obtain for $\hat{\mathbf{x}}(s)$

$$\hat{x}(s) = s, \quad \hat{y}(s) = \int_0^s ds' v_y\left[\hat{\mathbf{x}}_0(s)\right] \tag{13}$$

The particle displacement $\mathbf{x}(t)$ in time is given by $\mathbf{x}(t) = \hat{\mathbf{x}}[s(t)]$. With $s(t) = \max[s|t(s) \le t]$, the longitudinal displacement can be written as

$$x(t) = \max[s\left|t(s) \le t\right] = \langle v \rangle t + \int_0^t dt' v_x'\left[\mathbf{x}_0\left(t'\right)\right], \tag{14}$$

where $\mathbf{x}_0(t) = (\langle v \rangle t, 0)^\top$. This formulation shows that the longitudinal particle motion is determined by the variability of travel time $t(s)$. The transverse displacement is given by

$$y(t) = \int_0^{\langle v \rangle t} ds' v_y[\mathbf{x}_0(s)] = \hat{y}(\langle v \rangle t). \tag{15}$$

It is determined by the variability of the spatial increment rather than the travel time.

3.1.1. Transverse Dispersion

We consider now the transverse increment process

$$\nu(s) = \sin[\alpha(s)] = \frac{v_y\left[\hat{\mathbf{x}}_0(s)\right]}{\langle v \rangle}, \tag{16}$$

where $\alpha(s)$ is the angle between the tangent of the streamline at distance s and the x-direction. In first-order perturbation theory, $\alpha(s) = \nu(s)$. That is, the statistic of $\nu(s)$ and $\alpha(s)$ are identical in this approximation. In order to determine their statistics, we first determine the statistics of $v_y(\mathbf{x})$. First-order perturbation theory in $Y(\mathbf{x})$ renders $v_y(\mathbf{x})$ as a linear functional of $Y(\mathbf{x})$ (Dagan, 1984),

$$v_y(\mathbf{x}) = \langle v \rangle \int_{-\infty}^{\infty} d\mathbf{x}' \kappa_y\left(\mathbf{x} - \mathbf{x}'\right) Y\left(\mathbf{x}'\right). \tag{17}$$

The kernel $\kappa_y(\mathbf{x})$ can be written as

$$\kappa_y(\mathbf{x}) = \frac{\partial^2 G(\mathbf{x})}{\partial x \partial y}, \quad G(\mathbf{x}) = -\frac{1}{2\pi}\ln(|\mathbf{x}|). \tag{18}$$

As $Y(\mathbf{x})$ is a Gaussian distributed random field, the linearity of relation (Equation 17) implies that $v_y(\mathbf{x})$ is also Gaussian distributed. Since $v_y(\mathbf{x})$ is a Gaussian random field, also $\nu(s)$ is Gaussian. Thus, they can be fully characterized by the mean, variance σ_ν^2 and correlation function $\rho_\nu(s) = \langle \nu(s'+s)\nu(s')\rangle/\sigma_\nu^2$. Its mean is $\langle \nu(s)\rangle = 0$, its variance is $\sigma_\nu^2 = \sigma_Y^2/8$ and its correlation function is $\rho_\nu(s) = f(s/\ell_Y)$ where (Hsu, 1999)

$$f(s) = \frac{72}{s^4} - \frac{4}{s^2} - 8\left(\frac{1}{s} + \frac{4}{s^2} + \frac{9}{s^3} + \frac{9}{s^4}\right)\exp(-s). \tag{19}$$

The increment process $\nu(s)$ is a stationary multi-Gaussian process. In other words, it is a correlated Gaussian noise. Thus, transverse particle motion describes the correlated random walk.

$$\frac{d\hat{y}(s)}{ds} = \nu(s). \tag{20}$$

The mean transverse displacement is $\langle \hat{y}(s)\rangle = 0$, and its variance $\hat{\sigma}_y^2(s)$ is

$$\hat{\sigma}_y^2(s) = 2\sigma_\nu^2 \int_0^s ds' \int_0^{s'} ds'' \rho_\nu(s''). \tag{21}$$

The double integral can be evaluated explicitly by inserting expression (Equation 19), which gives (Dagan, 1988)

$$\hat{\sigma}_y^2(s) = \sigma_Y^2 \ell_Y^2 \left[\ln(s/\ell_Y) - \frac{3}{2} + \gamma + E_1(s/\ell_Y) + \frac{\ell_Y^2}{s^2} - \frac{3\ell_Y^2 \exp(-s/\ell_Y)(1+s/\ell_Y)}{s^2}\right]. \tag{22}$$

where γ is the Euler-Mascheroni constant and $E_1(t)$ the exponential integral (Abramowitz & Stegun, 1972). The displacement variance $\sigma_y^2(t)$ is obtained according to Equation 15 by setting $s = \langle v\rangle t$ in Equation 22. In the limit $s \ll 1$, Equation 22 is quadratic in s,

$$\hat{\sigma}_y^2(s) = \sigma_v^2 s^2. \tag{23}$$

For distances $s \gg \ell_Y$, it evolves as

$$\hat{\sigma}_y^2(s) = \sigma_Y^2 \ell_Y^2 \ln(s/\ell_Y). \tag{24}$$

It grows with the logarithm of time, that is, it shows ultraslow diffusion, which is due to the transverse confinement of the streamlines of the flow field. Figure 2 shows the evolution of $\sigma_y(t)$ given by Equation 22 for $s = \langle v\rangle t$. The

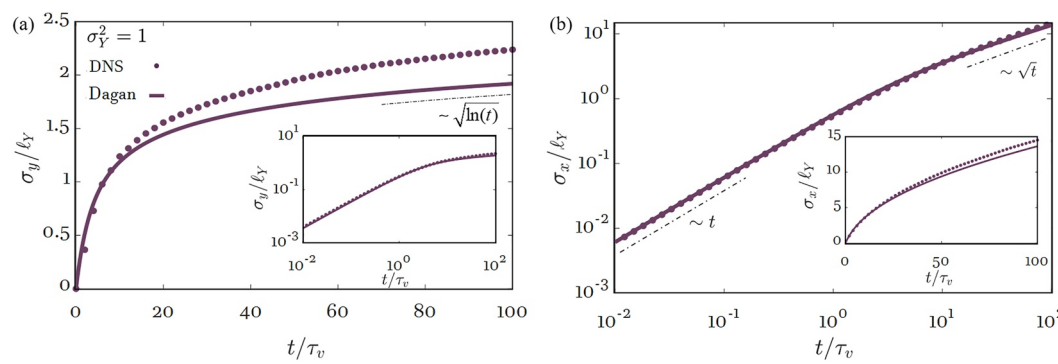

Figure 2. Time behavior of (a) the transverse σ_y (insert in logarithmic scale) and (b) longitudinal dispersive scale σ_x (insert in linear scale) considering results grounded on the direct numerical simulation (direct numerical simulation [DNS]—symbols) and the perturbation theory solution of Dagan, Equations 22 and 30 (Dagan—solid curves), for a mildly degree of heterogeneity, that is, $\sigma_Y^2 = 1$.

perturbation theory expression is compared to direct numerical simulations for $\sigma_Y^2 = 1$. While the perturbation theory provides a good description of the overall evolution of $\sigma_y(t)$, it underestimates $\sigma_y(t)$ for times larger than τ_v. Nevertheless, the data confirms the predicted asymptotic $\ln(t)$ scaling of $\sigma_y^2(t)$.

3.1.2. Streamwise Dispersion

For completeness, we provide here also the perturbation theory results for streamwise dispersion. The streamwise velocity $v_x(\mathbf{x})$ is given in perturbation theory by (Dagan, 1984)

$$v_x'(\mathbf{x}) = \langle v \rangle \int_{-\infty}^{\infty} d\mathbf{x}' \kappa_x(\mathbf{x} - \mathbf{x}') Y(\mathbf{x}'), \tag{25}$$

where the kernel $\kappa_x(\mathbf{x})$ is defined by

$$\kappa_x(\mathbf{x}) = \delta(\mathbf{x}) - \frac{\partial^2 G(\mathbf{x})}{\partial x^2}. \tag{26}$$

Thus, $v_x(\mathbf{x})$ is a correlated Gaussian random field. As a consequence, the Lagrangian velocity fluctuation $w_x'(t) \equiv v_x[\mathbf{x}_0(t)]$ is a correlated Gaussian process and $x(t)$ satisfies the correlated random walk

$$\frac{dx(t)}{dt} = \langle v \rangle + w_x'(t). \tag{27}$$

The mean of $w_x'(t)$ is zero and its variance is given by $\sigma_{w_x}^2 = 3\langle v^2 \rangle \sigma_Y^2/8$. Its correlation function is $\rho_{w_x}(t) = g(t/\tau_v)$ with (Hsu, 1999)

$$g(t) = \left\{ \frac{20}{3}\frac{1}{t^2}\left[1 - (1+t)\exp(-t)\right] - \frac{12}{3}\left[\frac{6}{t^4} - \left(\frac{6}{t^4} + \frac{6}{t^3} + \frac{3}{t^2} + \frac{1}{t}\right)\exp(-t)\right] \right\}. \tag{28}$$

The streamwise displacement variance is given by

$$\sigma_x^2(t) = 2\sigma_{w_x}^2 \int_0^t dt' \int_0^{t'} dt'' \rho_{w_x}(t''). \tag{29}$$

Explicit evaluation of the double integral using expression (Equation 28) gives (Dagan, 1988)

$$\sigma_x^2(t) = \sigma_Y^2 \langle v \rangle \ell_Y \left[2t/\tau_v - 3\ln(t/\tau_v) + \frac{3}{2} - 3\gamma - E_1(t/\tau_v) + \frac{\tau_v^2 \exp(-t/\tau_v)(1 + t/\tau_v) - 1}{t^2} \right]. \tag{30}$$

Figure 2 shows the evolution of $\sigma_x(t)$ from Equation 30. Also here, the perturbation theory expression is a good quantitative descriptor for overall evolution of σ_x^2, but underestimates the numerical data at asymptotic times. In the following, we discuss a stochastic TDRW model to describe solute dispersion for strong spatial heterogeneity.

3.2. Stochastic Time-Domain Random Walk

We use a stochastic time-domain random approach to quantify particle motion at large spatial heterogeneity. The TDRW approach models particle motion at equidistant displacements along streamlines based on Equation 6. This approach has been used to quantify streamwise particle transport, that is, arrival time distributions, streamwise concentration profiles, and displacement moments in porous and fractured media (Comolli et al., 2019; Hyman et al., 2019; Kang et al., 2011; Painter et al., 2008). In the following, we briefly recapitulate the modeling of streamwise particle motion using the approach of Comolli et al. (2019), before we analyze the dynamics of transverse motion.

3.2.1. Streamwise Motion

The streamwise motion of solute particles is described by the following set of equations (Comolli et al., 2019; Dentz et al., 2016),

$$\frac{dx(s)}{ds} = \chi^{-1}, \quad \frac{dt(s)}{ds} = \frac{1}{v_s(s)}, \tag{31}$$

where χ denotes the advective tortuosity (Koponen et al., 1996), which is defined as

$$\chi = \frac{\langle v_e \rangle}{\langle v \rangle} = \frac{1}{\langle \cos[\alpha(s)] \rangle}, \tag{32}$$

The analysis of Hakoun et al. (2019) for two-dimensional Darcy-scale heterogeneous porous media showed that the series of equidistant particle speeds $\{v_s(s)\}$ can be modeled in terms of an Ornstein-Uhlenbeck process for the normal scores transform $\omega(s)$ of $v_s(s)$. The normal score transform is defined as

$$\omega(s) = \Phi^{-1}\{P_s[v(s)]\}, \tag{33}$$

where $\Phi(w)$ is the cumulative unit Gaussian distribution, and $\Phi^{-1}(s)$ its inverse, $P_s(v)$ is the cumulative distribution of $v_s(s)$. The normal score transform $\omega(s)$ satisfies

$$\frac{d\omega(s)}{ds} = -\frac{\omega(s)}{\ell_c} + \sqrt{\frac{2}{\ell_c}}\eta(s), \tag{34}$$

where ℓ_c denotes the correlation length, and $\eta(s)$ is a Gaussian white with zero mean and covariance $\langle \eta(s)\, \eta(s') \rangle = \delta(s - s')$. Using Monte Carlo simulations for the same numerical setup as used in this paper, Hakoun et al. (2019) found the following empirical relationship between ℓ_c and the statistics of the underlying hydraulic conductivity field (see also Table 1),

$$\ell_c = \ell_Y \left(0.181\sigma_Y^2 + 2.221\right). \tag{35}$$

This regression is consistent with the prediction $\ell_c = 8\ell_Y/3$ of perturbation theory (Cvetkovic et al., 1996).

3.2.2. Transverse Motion

Here, we analyze transverse particle motion in order to understand and quantify its stochastic dynamics. The equation of motion of solute particles in direction transverse to the mean flow can be written as

$$\frac{d\hat{y}(s)}{ds} = \sin[\alpha(s)]. \tag{36}$$

In order to probe the transverse motion, we analyze the distribution of $\alpha(s)$ sampled along and across trajectories

$$p_\alpha(a) = \frac{1}{V_0}\int_{\Omega_0} d\mathbf{x}_0 \frac{1}{L}\int_0^L ds' \delta\left[a - \alpha\left(s', \mathbf{x}_0\right)\right], \tag{37}$$

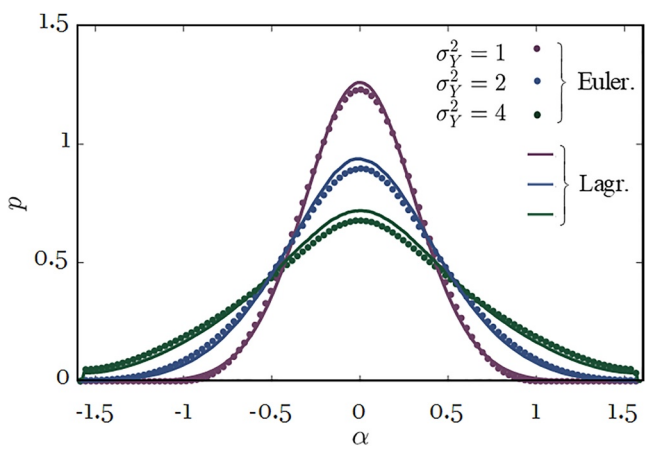

Figure 3. Probability distribution of the angle α obtained from (circles) spatial sampling and (solid lines) equidistant sampling along streamlines for $\sigma_Y^2 = (1, 2, 4)$.

where $\alpha(s, \mathbf{x}_0)$ denotes the angle along the trajectory that starts at $\mathbf{x}_0$, Ω_0 the set of initial points and V_0 its volume. We assume that the distribution is stationary, that is, it does not depend on s. We also consider sampling of the angle $\alpha(\mathbf{x})$ in space,

$$p'_\alpha(a) = \frac{1}{V}\int_\Omega d\mathbf{x}\delta[a - \alpha(\mathbf{x})]. \tag{38}$$

Figure 3 shows that the two sampling methods give approximately the same distribution, which indicates that the angle α is independent from the velocity. This observation is consistent with the findings of Meyer et al. (2013).

The distribution $p_\alpha(a)$ has zero mean and is symmetric around zero. In fact, as shown in Section 3.1, perturbation theory indicates that for low degree of heterogeneity $\alpha(s)$ is Gaussian distributed with variance $\sigma_\alpha^2 = \sigma_Y^2/8$. Figure 4a suggests that for increasing disorder, $p_\alpha(a)$ follows a Gaussian distribution that is wrapped around the unit circle, that is, a wrapped Gaussian distribution (Fisher, 1993). In Figure 4, data for the angle distribution is compared

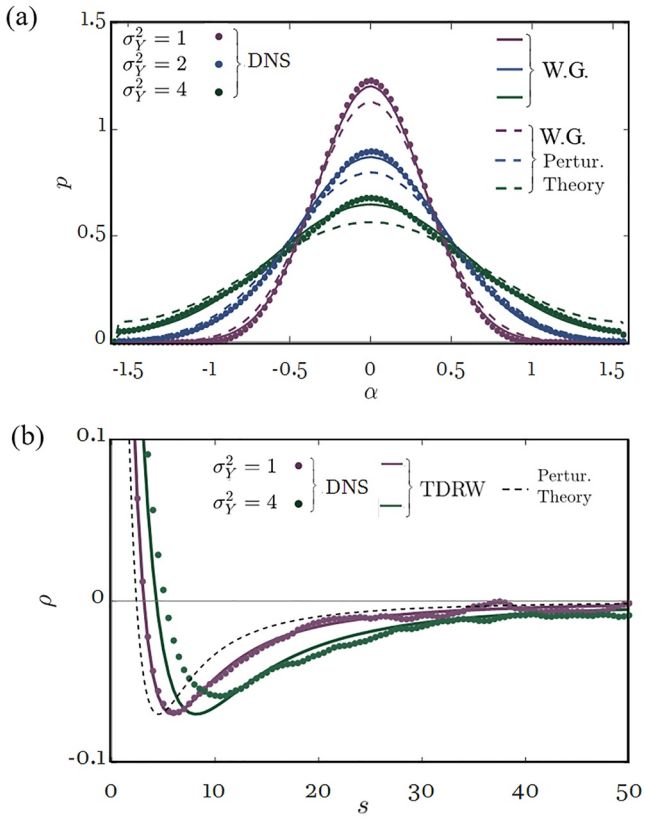

Figure 4. (a) Probability distribution of $\alpha(s)$ grounded on (circles) the direct numerical simulation (DNS), wrapped Gaussian distributions with σ_α^2 parameterized by (dashed lines) perturbation theory and (solid lines) by the Eulerian statistics of α, for $\sigma_Y^2 = (1, 2, 4)$. (b) Correlation function of $\alpha(s)$ from (circles) DNS (black dashed line), perturbation theory, and (solid lines) perturbation theory with adjusted correlation length ℓ_α, for $\sigma_Y^2 = (1, 4)$ (results for $\sigma_Y^2 = 2$ are in between).

with the wrapped Gaussian distribution. While perturbation theory provides a good estimate for the shape of $p_\alpha(x)$, it overestimates the width of $p_\alpha(a)$ for increasing σ_Y^2. Thus, we adjust σ_α^2 on the base of the Eulerian statistics of the angle α, see previous discussion of Figure 3.

Furthermore, we consider the Lagrangian correlation function of $\alpha(s)$, which is defined by

$$\rho_\alpha(s) = \frac{1}{\sigma_\alpha^2 V_0} \int_{\Omega_0} d\mathbf{x}_0 \frac{1}{L} \int_0^L ds' \alpha(s + s', \mathbf{x}_0) \alpha(s', \mathbf{x}_0). \tag{39}$$

Again, we assume that the statistics are stationary. As shown in Section 3.1, perturbation theory indicates that $\rho_\alpha(s)$ is indeed stationary and given by $\rho_\alpha(s) = f(s/\ell_Y)$, where $f(s)$ is given by Equation 19. Figure 4b shows $\rho_\alpha(s)$ for different σ_Y^2. The correlation decays sharply at short distances and becomes negative for distances larger than ℓ_Y, that is, at larger distances, angles are persistently anticorrelated. Note that, expression (Equation 19) embeds these features while there is a quantitative mismatch with the numerical data. Thus, for increasing σ_Y^2, we represent the correlation function by Equation 19 as

$$\rho_\alpha(s) = f(s/\ell_a), \tag{40}$$

where the correlation length ℓ_a is adjusted from the tail of the empirical Lagrangian correlation function to capture the long-range anticorrelation. Based on these observations, in the following, we first pose a Markov model for the evolution of the angle, and then a long-range correlated model.

3.2.3. Ornstein-Uhlenbeck Process

Based on the observation that the correlation function $\rho_\alpha(s)$ decays rapidly to zero with lag-distance s, and that its distribution is Gaussian, we pose an Ornstein-Uhlenbeck process for $\alpha(s)$ that has both these properties. Thus, the angle follows the Langevin equation

$$\frac{d\alpha(s)}{ds} = -\frac{\alpha(s)}{\ell_\alpha} + \sqrt{2\frac{\sigma_\alpha^2}{\ell_\alpha}}\eta(s), \tag{41}$$

where ℓ_α denotes a characteristic fluctuation scale of $\alpha(s)$. In this approach, the correlation function $\rho_\alpha(s)$ is exponential (Gardiner, 1986),

$$\rho_\alpha(s) = \exp(-|s|/\ell_\alpha). \tag{42}$$

In order to assess, the validity of this approach, we compare it to the perturbation theory results for the displacement variance $\hat{\sigma}_y^2(s)$ for $s \gg \ell$. Equation 24 indicates that $\hat{\sigma}_y^2(s) \sim \ln(s/\ell_Y)$ increases with the logarithm of distance s. For weak heterogeneity, that is, $\sigma_\alpha^2 \ll 1$, the transverse displacement can be approximated by

$$\frac{d\hat{y}(s)}{ds} = \alpha(s), \tag{43}$$

and the correlation length is $\ell_\alpha = \ell_Y$. Using expression (Equation 42) in Equation 21 gives for $s \gg \ell_Y$

$$\hat{\sigma}_y^2(s) = 2\sigma_\alpha^2 \ell_Y s. \tag{44}$$

It increases linearly with distance. Thus, the asymptotic behavior of the Markov model (Equation 41) is not compatible with the true behavior for purely advective transport at large distances. While the behavior predicted by Equation 44 may be compatible with transverse dispersivities observed under realistic aquifer conditions

and finite Pe, it does not reproduce the transverse dispersion behavior predicted for purely advective transport (Attinger et al., 2004; Dagan, 1989).

3.2.4. Stationary Correlated Gaussian Process

Careful inspection of $\rho_\alpha(s)$ in Figure 4b reveals that after the sharp initial decrease of the correlation function, a persistent degree of anticorrelation emerges. The latter is a fundamental aspect of transverse motion, and is a consequence of the solenoidal character of the flow field, that is, $\nabla \cdot \mathbf{q} = 0$. This property leads to the meandering of the streamlines as shown in Figure 1.

It is important to note that the negative values of $\rho_\alpha(s)$ are small. That is, while particles tend to persistently change the transverse direction, the magnitudes of the transverse excursions are only weakly correlated. In other words, the asymmetry of $\rho_\alpha(s)$ in terms of streamwise persistence and intensity of the anticorrelation are the key elements underpinning the limitation of particle motion in the transverse direction that manifests ultraslow transverse dispersion as expressed by Equation 24. As shown in Section 3.1, perturbation theory indicates that the angle process $\alpha(s)$ can be described as a stationary correlated Gaussian noise. In full analogy, for large disorder variance, we also model $\alpha(s)$ as a correlated Gaussian process characterized by the correlation function (Equation 40).

To generate trajectories of $\alpha(s)$, it is convenient to introduce the covariance function of α, which is defined by $C_\alpha(s) = \sigma_\alpha^2 \rho_\alpha(s)$. The covariance function can be expanded as

$$C_\alpha(s) = \sum_{n=1}^{\infty} \lambda_n \phi_n(s), \tag{45}$$

where the $\phi_n(s)$ are the eigenfunctions and the λ_n the respective eigenvalues of $C_\alpha(s)$ (Dell'Oca & Porta, 2020; D. Zhang & Lu, 2004). Thus, the stochastic process $\alpha(s)$ can be represented by the Karhunen-Loève expansion

$$\alpha(s) = \sum_{n=1}^{\infty} \sqrt{\lambda_n} \phi_n(s) \xi_n, \tag{46}$$

where the ξ_n are independent identically distributed Gaussian random variables of zero mean and unit variance. The numerical implementation is detailed in Appendix A.

4. Transport Behaviors

In this section, we compare the predictions of the stochastic TDRW model with data from direct numerical simulations for the longitudinal and transverse dispersive scales, streamwise and transverse particle distribution, as well as the full two-dimensional particle distributions. The direct flow and transport simulations are described in Section 2.3. We consider media characterized by $\sigma_Y^2 = (1, 2, 4)$.

The model parameters χ and σ_α^2 of the stochastic TDRW model are fully constrained by the Eulerian flow properties. The correlation legnth ℓ_c is given by the regression in Equation 35. The correlation length ℓ_α is adjusted from the Lagrangian correlation function as outlined in Section 3.2.2. Table 1 lists the values of ℓ_c, χ, σ_α^2 and ℓ_α for the different values of σ_Y^2.

Table 1
Values of Model Parameters in the Two-Dimensional Stochastic Time-Domain Random Walk Approach

σ_Y^2	χ	σ_α^2	ℓ_c	ℓ_α
1	1.06	0.11	2.4	1.28
2	1.1	0.21	2.58	1.4
4	1.2	0.38	2.95	1.8

4.1. Spatial Variance

Figure 5 shows the time behavior of the streamwise and transverse dispersion scales σ_x and σ_y from the direct numerical simulations and the stochastic TDRW model. In agreement with Comolli et al. (2019), the stochastic TDRW describes the full temporal evolution of σ_x including the ballistic regimes for $t < \tau_v$, in which $\sigma_x(t) \sim t$, and the cross-over from ballistic to the asymptotic behaviors $\sigma_x \sim \sqrt{t}$ at times $t \gg \tau_v$.

The stochastic TDRW model captures also the full time evolution of $\sigma_y(t)$ including the early time ballistic regime and the transition to ultraslow diffusion at times $t \gg \tau_v$. The strong increase of σ_y at intermediate times reflects

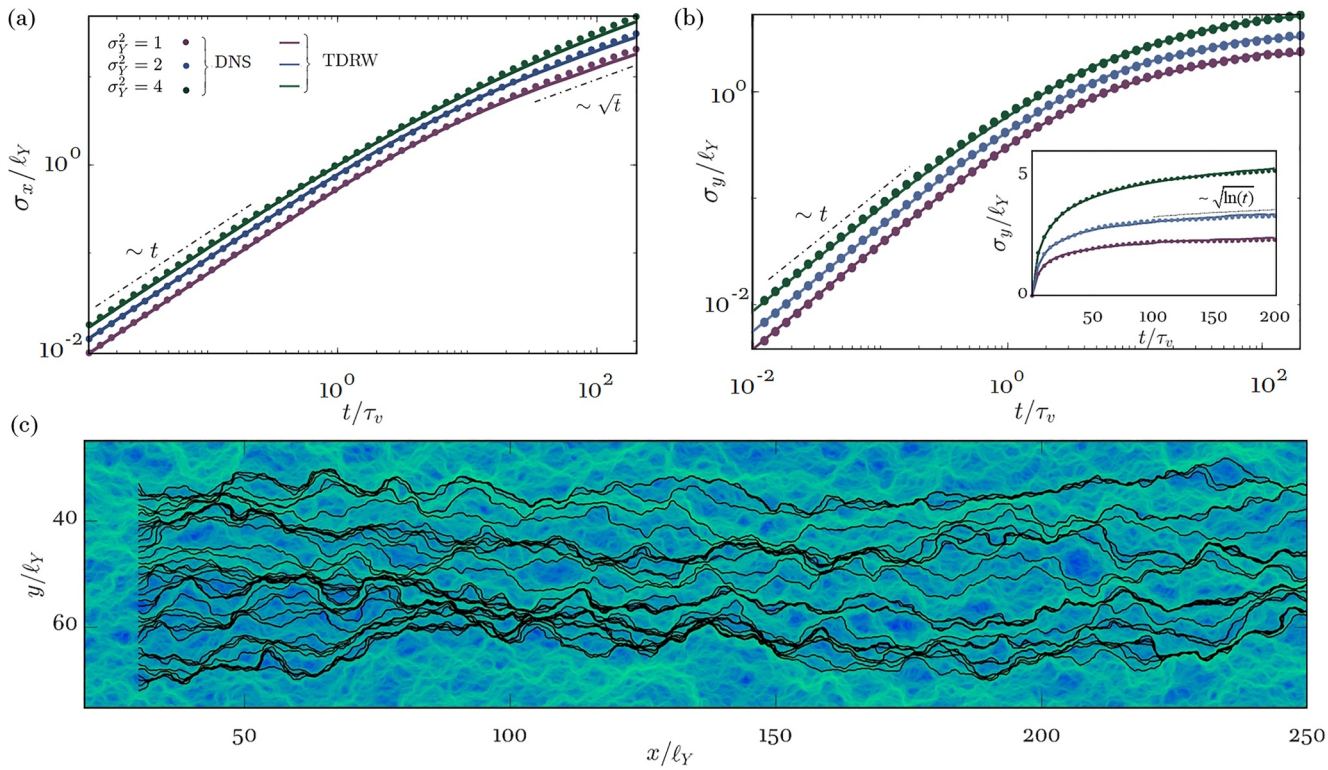

Figure 5. Time behavior of (a) the longitudinal σ_x and (b) the transverse σ_y (inset bilinear scale) dispersion scales for $\sigma_Y^2 = (1, 2, 4)$. (c) Samples of particle trajectories (black curves) released in a Darcy' flow field (v, logarithmic scale, blue low and green high) for $\sigma_Y^2 = 4$: focusing of the trajectories in the nearest set of preferential flow paths underpins the intense growth of $\sigma_y(t)$ at middle times ($\mathcal{O}(t) \sim (1 - 10)\tau_v$), while the meandering of the trajectories sustains the logarithmic growth of $\sigma_y(t)$ at the large-scale ($\mathcal{O}(t) \sim 100\tau_v$).

the focusing of solute particles from their initial positions into flow channels as illustrated in Figure 5c. For later times, the transverse displacement is determined by the meandering of these flow channels, see Figures 1 and 5c. This meandering confines transverse motion at large-scale, which is here qualitatively and quantitatively reproduced by the stochastic TDRW model.

4.2. Particle Distributions

In addition to the dispersion scales, we consider now the longitudinal and transverse particle distributions. Figure 6 depicts snapshots of $p(x, t)$ and $p(y, t)$ at different times. For $p(y, t)$, only the positive branch of the symmetric distribution is shown.

Figures 6a, 6c, and 6e show satisfactory agreement between the numerical data for $p(x, t)$ and the stochastic TDRW model, which is able to reproduce the full transition from initially skewed to asymptotic Gaussian behavior for moderately to strongly heterogeneous media.

Figures 6b, 6d, and 6f highlight the satisfactory agreement between the numerical data for $p(y, t)$ and the stochastic TDRW model from early to late times, and for all degrees of heterogeneity under consideration. We observe a rapid expansion of $p(y, t)$ at the early times (e.g., $t = (1, 5, 10)\tau_v$), that is, as the solute particles tend to be focused toward the nearest flow channels such that larger absolute values of y become more likely. As time passes ($t = (20, 50, 100, 200)\tau_v$), solute particles travel within flow channels characterized by a meandering structure which underpins the decreasing rate of expansion of $p(y, t)$, consistent with the behavior of $\sigma_y(t)$ shown in Figure 5. Note that, $p(y, t)$ tends toward Gaussianity at late times (e.g., $t = (100, 200)\tau_v$). Gotovac et al. (2009) considered the transverse particle distribution after fixed travel distances and found that it approaches Gaussianity already after relatively short distances of about $5\ell_Y$. Our results for the distribution of $\hat{y}(s)$ after fixed travel distances s (not shown) confirm these findings.

Finally, we consider the joint distribution $p(\mathbf{x}, t)$ of streamwise and transverse particle positions at different times. Figure 7 depicts $p(\mathbf{x}, t)$ from the numerical data in the upper half of each panel, and the stochastic TDRW model

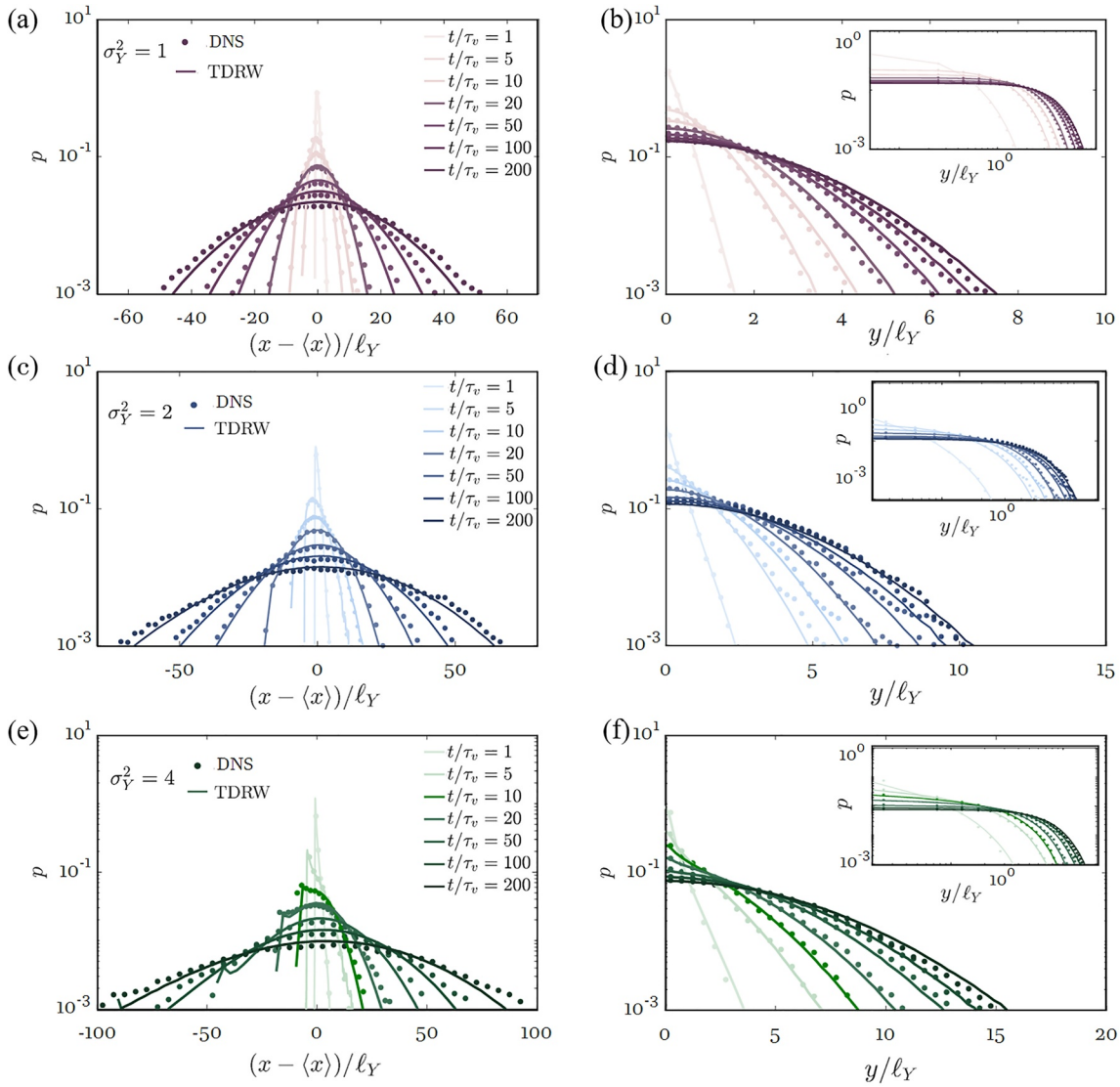

Figure 6. Probability distribution of particle position along the longitudinal, that is, $p(x, t)$, and transverse, that is, $p(y, t)$ (only the positive branch of the symmetric distribution is depicted), directions at diverse times considering (a, d) $\sigma_Y^2 = 1$, (b, e) $\sigma_Y^2 = 2$ and (c, f) $\sigma_Y^2 = 4$. Results based on the (symbols) direct numerical simulations and (solid lines) time-domain random walk (TDRW) are depicted.

in the lower half, at times $t = (5, 20, 50)\tau_v$ for $\sigma_Y^2 = 1, 2, 4$. We find an overall satisfactory agreement between the numerical data and the stochastic TDRW model, which corroborates the assumption of treating the streamwise longitudinal and transverse transport as two independent stochastic processes (Meyer & Tchelepi, 2010; Meyer et al., 2013).

5. Conclusions

The current study is motivated by the scientific challenge of defining a stochastic model that quantifies (non-Fickian) ensemble solute dispersion both along the direction parallel and transverse to the mean flow.

With this objective in mind, we analyze the stochastic dynamics of two-dimensional particle motion in Darcy-scale heterogeneous porous media. The spatial variability of the hydraulic conductivity is represented using a stochastic modeling approach such the $K(\mathbf{x})$ is a realization of a lognormally distributed multi-Gaussian spatial random field. The Lagrangian particle dynamics are analyzed through numerical particle tracking simulations as well as perturbation theory by using an equidistant sampling strategy, which acknowledges the spatial organization of the

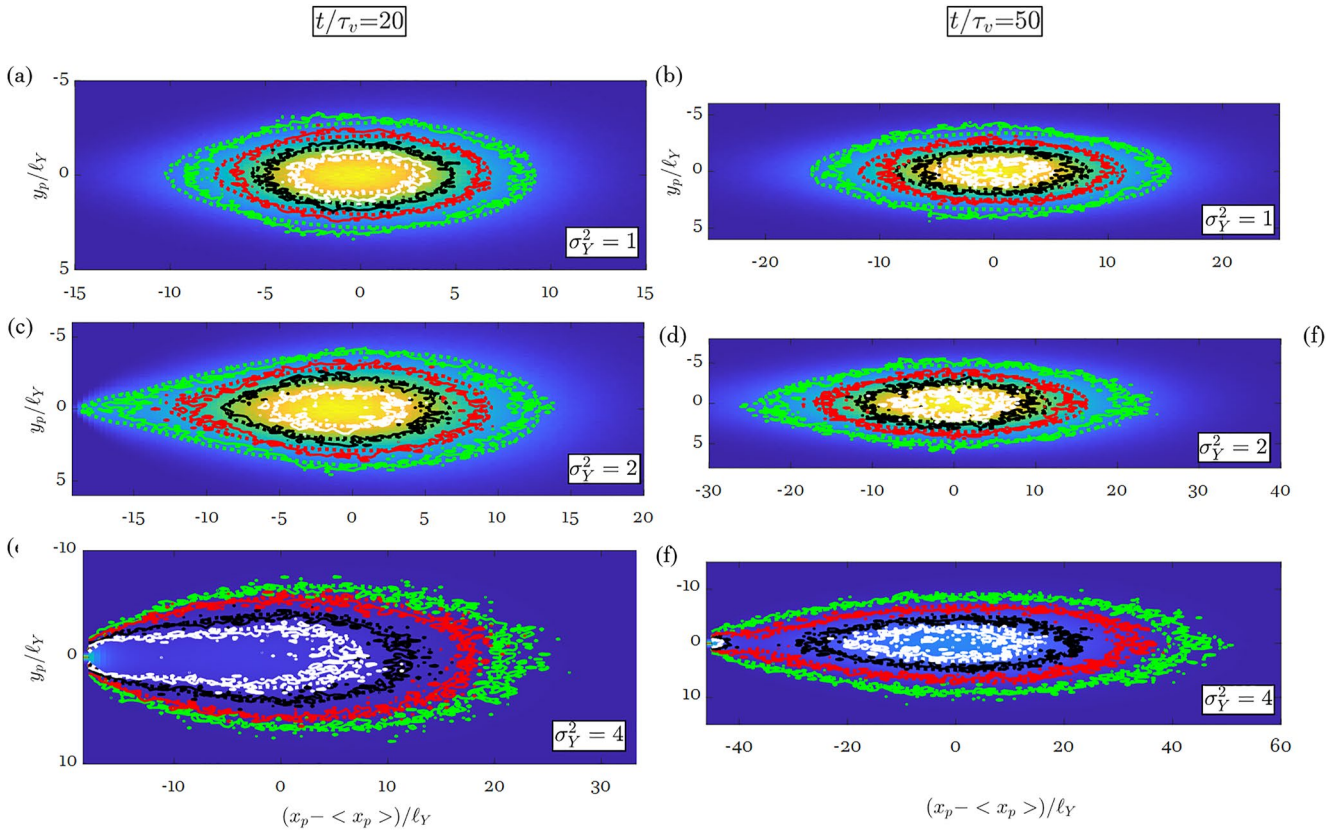

Figure 7. Joint probability distribution of particles locations $p(\mathbf{x}, t)$ at times $t = (20, 50)$ and for diverse degree of formation heterogeneity (a, b) $\sigma_Y^2 = 1$, (c, d) $\sigma_Y^2 = 2$ and (e, f) $\sigma_Y^2 = 4$. The colormap shows the TDRW data (blue low, yellow high). For each pannel, iso-probability contours are drawn considering the TDRW (dashed curves) and the direct numerical simulation (DNS) (continuous curves) results.

Eulerian and Lagrangian flow velocities on a characteristic length scale. The perturbation theory analysis reveals that longitudinal particle motion is determined by the variability of travel times along streamlines, while transverse motion is determined by the fluctuation structure of transverse displacements. The former can be captured by a Markov model for the equidistantly sampled flow speeds, that is, flow speeds are only weakly correlated. The latter, however, turns out to be persistently anticorrelated as a consequence of the solenoidal character of the flow field. This strong anticorrelation leads to an ultraslow growth of the transverse displacement variance with distance and time. The transverse displacements are characterized by the series of angles between the streamlines and the mean flow direction. Perturbation theory shows that the angle distribution can be represented by a wrapped Gaussian distribution, which is valid also for increasing heterogeneity strength. Unlike the speed series, the angle series cannot be represented as a Markov process. The angular increments are modeled as a correlated Gaussian noise, which renders the angle process as a correlated Brownian motion. The Gaussian increment process is generated here using a Karhunen-Loeve expansion. For low medium heterogeneity, the model can be fully constrained by medium and flow properties using perturbation theory. For increasing heterogeneity, the model can be constrained by Eulerian flow statistics and the characteristic length scale of the fluctuations of the Lagrangian angular series.

The proposed stochastic TDRW model combines a Markov model for the particle speeds with a correlated Gaussian noise for transverse particle displacements. Comparison with detailed numerical simulations for the longitudinal and transverse dispersion scales and the full particle distributions shows that the model captures the dynamics of advective particle motion both qualitatively and quantitatively. This underpins the critical importance of correctly representing the topological constraints of the underlying Eulerian flow field in the large-scale particle dynamics in two-dimensional steady-state Darcy's flows (Lester et al., 2021, 2022). These behaviors cannot be accounted for by two-dimensional TDRW or CTRW schemes that model transverse displacements as Markov processes. The proposed stochastic TDRW model is able to quantify large-scale longitudinal and

transverse advective particle motion in two-dimensional divergence-free Darcy flows, which occur, for example, in shallow aquifers and rough fractures. The correct representation of transverse ensemble dispersion facilitates the assessment of the overlap of solute plumes that originate from adjacent point sources, and thus for the assessment of the concentration content of a mixture (Dentz et al., 2022). Furthermore, for a small initial plume, transverse motion determines the area swept by the plume as it migrates through the medium, and the uncertainty of the plume position.

The results of the proposed stochastic TDRW are strictly valid for two-dimensional formations and therefore of relevance for flow and transport in (quasi) two-dimensional heterogeneous media such as rough fractures and shallow aquifers. At the same time, it is not straightforward to transfer the results to dispersion in three-dimensional porous media because, in general, the streamlines in three-dimensional formations can braid sustaining the linear scaling of the variance of purely advective particles at the large-scale in contrast with the ultraslow regime found in two-dimensional systems (Fiori & Jankovic, 2012; Lester et al., 2022). On the other hand, the proposed framework can be applied to flow and transport in three dimensions, that is, the nature of the correlation of solute velocities and orientations for three-dimensional porous formations could inform the stochastic model for particle motion in the two transverse directions as proposed in the current work.

Appendix A: Generation of Long-Range Correlated Stochastic Angle Series

The eigenvalues λ_n and eigenfunctions $\phi_n(s)$ of the covariance function $C_\alpha(s)$ are obtained from the following Fredholm equation

$$\int_0^\infty C_\alpha(s-s')\phi_n(s')ds' = \lambda_n\phi_n(s). \tag{A1}$$

For general $C_\alpha(s)$, Equation A1 can be solved numerically as outlined in the following. First, we discretize s into N intervals of length Δs such that $s_i = i\Delta s$. Then, we define the symmetric $N \times N$ covariance matrix C_{ij} as

$$C_{ij} = C_\alpha(s_i - s_j)\Delta s. \tag{A2}$$

The eigenfunctions are discretized as $\phi_i^{(n)} = \phi_n(s_i)$ and are represented by the eigenvectors $\boldsymbol{\phi}^{(n)}$. The angle process is discretized as $\alpha_i = \alpha(s_i)$ and represented by the vector $\boldsymbol{\alpha}$.

The discrete version of Equation A1 is

$$\mathbf{C}\boldsymbol{\phi}^{(n)} = \lambda_n\boldsymbol{\phi}^{(n)}. \tag{A3}$$

The eigenvalues of $\mathbf{C}$ are obtained from

$$\det(\mathbf{C} - \lambda\mathbb{I}) = 0, \tag{A4}$$

where $\mathbb{I}$ is the identity matrix. The eigenvector $\boldsymbol{\phi}^{(n)}$ corresponding to the nth eigenvalue λ_n is obtained by solving Equation A3. Thus realizations of the correlated Gaussian process $\boldsymbol{\alpha}$ are generated according to the discrete version of Equation 46 as

$$\boldsymbol{\alpha} = \sum_{n=1}^{N_\lambda} \sqrt{\lambda_n}\boldsymbol{\phi}^{(n)}\xi_n. \tag{A5}$$

Here, we set $N_\lambda = 1{,}000 < N$ modes. Furthermore, we set $\Delta s = l_Y/10$ and $N = 5{,}000$. The computation of the eigenvalues and eigenvectors is carried out with standard commands in MATLAB (MathWorks, 2015).

Data Availability Statement

The computational data and codes for data analysis supporting this work are available upon request and at the open-access repository (Dell'Oca & Dentz, 2023). We thank Olaf Cirpka, Aldo Fiori, and an anonymous reviewer for valuable comments and suggestions.

Acknowledgments
We acknowledge funding from the European Union's Horizon 2020 research and innovation programme under the H2020-MSCA-IF-2019 scheme with the grant agreement No. 895152 (MixUQ). M.D. acknowledges the support of the Spanish Research Agency (10.13039/501100011033), Spanish Ministry of Science and Innovation through grants CEX2018-000794-S and HydroPore PID2019-106887GB-C31. A.D. gratefully acknowledges P. Ackerer for sharing the numerical code for the flow problem.

References

Abramowitz, M., & Stegun, I. A. (1972). *Handbook of mathematical functions*. Dover Publications.
Adams, E. E., & Gelhar, L. W. (1992). Field study of dispersion in a heterogeneous aquifer: 2. Spatial moments analysis. *Water Resources Research*, *28*(12), 3293–3307. https://doi.org/10.1029/92wr01757
Attinger, S., Dentz, M., & Kinzelbach, W. (2004). Exact transverse macro dispersion coefficients for transport in heterogeneous porous media. *Stochastic Environmental Research and Risk Assessment*, *18*(1), 9–15. https://doi.org/10.1007/s00477-003-0160-6
Bear, J. (1972). *Dynamics of fluids in porous media*. American Elsevier.
Bellin, A., Salandin, P., & Rinaldo, A. (1992). Simulation of dispersion in heterogeneous porous formations: Statistics, first-order theories, convergence of computations. *Water Resources Research*, *28*(9), 2211–2227. https://doi.org/10.1029/92wr00578
Bénichou, O., & Oshanin, G. (2002). Ultraslow vacancy-mediated tracer diffusion in two dimensions: The Einstein relation verified. *Physical Review E—Statistical Physics, Plasmas, Fluids, and Related Interdisciplinary Topics*, *66*(3), 031101. https://doi.org/10.1103/physreve.66.031101
Benson, D. A., Wheatcraft, S. W., & Meerschaert, M. M. (2000). Application of a fractional advection-dispersion equation. *Water Resources Research*, *36*(6), 1403–1412. https://doi.org/10.1029/2000wr900031
Berkowitz, B., Cortis, A., Dentz, M., & Scher, H. (2006). Modeling non-Fickian transport in geological formations as a continuous time random walk. *Reviews of Geophysics*, *44*(2). https://doi.org/10.1029/2005rg000178
Bijeljic, B., Mostaghimi, P., & Blunt, M. J. (2011). Signature of non-Fickian solute transport in complex heterogeneous porous media. *Physical Review Letters*, *107*(20), 204502. https://doi.org/10.1103/physrevlett.107.204502
Boettcher, S., & Sibani, P. (2011). Ageing in dense colloids as diffusion in the logarithm of time. *Journal of Physics: Condensed Matter*, *23*(6), 065103. https://doi.org/10.1088/0953-8984/23/6/065103
Comolli, A., Hakoun, V., & Dentz, M. (2019). Mechanisms, upscaling, and prediction of anomalous dispersion in heterogeneous porous media. *Water Resources Research*, *55*(10), 8197–8222. https://doi.org/10.1029/2019wr024919
Cvetkovic, V., Cheng, H., & Wen, X. H. (1996). Analysis of nonlinear effects on tracer migration in heterogeneous aquifers using Lagrangian travel time statistics. *Water Resources Research*, *32*(6), 1671–1680. https://doi.org/10.1029/96wr00278
Cvetkovic, V., Fiori, A., & Dagan, G. (2014). Solute transport in aquifers of arbitrary variability: A time-domain random walk formulation. *Water Resources Research*, *50*(7), 5759–5773. https://doi.org/10.1002/2014wr015449
Dagan, G. (1984). Solute transport in heterogeneous porous formations. *Journal of Fluid Mechanics*, *145*(1), 151–177. https://doi.org/10.1017/S0022112084002858
Dagan, G. (1988). Time-dependent macrodispersion for solute transport in anisotropic heterogeneous aquifers. *Water Resources Research*, *24*(9), 1491–1500. https://doi.org/10.1029/WR024i009p01491
Dagan, G. (1989). *Flow and transport in porous formations*. Springer.
de Dreuzy, J.-R., Beaudoin, A., & Erhel, J. (2007). Asymptotic dispersion in 2D heterogeneous porous media determined by parallel numerical simulations. *Water Resources Research*, *43*(10). https://doi.org/10.1029/2006wr005394
Dell'Oca, A., & Dentz, M. (2023). Dataset for stochastic dynamics of two-dimensional particle motion in Darcy-scale heterogeneous porous media [Dataset]. Authorea. https://doi.org/10.17632/2bkc7gp2sd
Dell'Oca, A., & Porta, G. M. (2020). Characterization of flow through random media via Karhunen–Loève expansion: An information theory perspective. *GEM-International Journal on Geomathematics*, *11*(1), 1–18. https://doi.org/10.1007/s13137-020-00155-x
Dell'Oca, A., Riva, M., Ackerer, P., & Guadagnini, A. (2019). Solute transport in random composite media with uncertain dispersivities. *Advances in Water Resources*, *128*, 48–58. https://doi.org/10.1016/j.advwatres.2019.04.005
Dell'Oca, A., Riva, M., Carrera, J., & Guadagnini, A. (2018). Solute dispersion for stable density-driven flow in randomly heterogeneous porous media. *Advances in Water Resources*, *111*, 329–345. https://doi.org/10.1016/j.advwatres.2017.10.040
Dentz, M., & Castro, A. (2009). Effective transport dynamics in porous media with heterogeneous retardation properties. *Geophysical Research Letters*, *36*(3), L03403. https://doi.org/10.1029/2008gl036846
Dentz, M., Comolli, A., Hakoun, V., & Hidalgo, J. J. (2020). Transport upscaling in highly heterogeneous aquifers and the prediction of tracer dispersion at the made site. *Geophysical Research Letters*, *47*(22), e2020GL088292. https://doi.org/10.1029/2020gl088292
Dentz, M., Cortis, A., Scher, H., & Berkowitz, B. (2004). Time behavior of solute transport in heterogeneous media: Transition from anomalous to normal transport. *Advances in Water Resources*, *27*(2), 155–173. https://doi.org/10.1016/j.advwatres.2003.11.002
Dentz, M., Hidalgo, J. J., & Lester, D. (2022). *Mixing in porous media: Concepts and approaches across scales* (pp. 1–49). Transport in Porous Media.
Dentz, M., Kang, P. K., Comolli, A., Le Borgne, T., & Lester, D. R. (2016). Continuous time random walks for the evolution of Lagrangian velocities. *Physical Review Fluids*, *1*(7), 074004. https://doi.org/10.1103/physrevfluids.1.074004
De Smedt, F., & Wierenga, P. J. (1984). Solute transfer through columns of glass beads. *Water Resources Research*, *20*(2), 225–232. https://doi.org/10.1029/wr020i002p00225
Deutsch, C. V., & Journel, A. G. (1992). *GSLIB: Geostatistical software library and user's guide*. Oxford University Press.
Domenico, P. A., & Schwartz, F. W. (1998). *Physical and chemical hydrogeology* (Vol. 506). Wiley.
Dünser, S., & Meyer, D. W. (2016). Predicting field-scale dispersion under realistic conditions with the polar Markovian velocity process model. *Advances in Water Resources*, *92*, 271–283. https://doi.org/10.1016/j.advwatres.2016.04.012
Edery, Y., Guadagnini, A., Scher, H., & Berkowitz, B. (2014). Origins of anomalous transport in heterogeneous media: Structural and dynamic controls. *Water Resources Research*, *50*(2), 1490–1505. https://doi.org/10.1002/2013wr015111
Fiori, A., Dagan, G., Jankovic, I., & Zarlenga, A. (2013). The plume spreading in the made transport experiment: Could it be predicted by stochastic models? *Water Resources Research*, *49*(5), 2497–2507. https://doi.org/10.1002/wrcr.20128
Fiori, A., & Janković, I. (2005). Can we determine the transverse macrodispersivity by using the method of moments? *Advances in Water Resources*, *28*(6), 589–599. https://doi.org/10.1016/j.advwatres.2004.09.009
Fiori, A., & Jankovic, I. (2012). On preferential flow, channeling and connectivity in heterogeneous porous formations. *Mathematical Geosciences*, *44*(2), 133–145. https://doi.org/10.1007/s11004-011-9365-2
Fiori, A., Zarlenga, A., Gotovac, H., Jankovic, I., Volpi, E., Cvetkovic, V., & Dagan, G. (2015). Advective transport in heterogeneous aquifers: Are proxy models predictive? *Water Resources Research*, *51*(12), 9577–9594. https://doi.org/10.1002/2015wr017118
Fisher, N. I. (1993). *Statistical analysis of circular data*. Cambridge University Press. Retrieved from https://www.cambridge.org/core/books/statistical-analysis-of-circular-data/324A46F3941A5CD641ED0B0910B2C33F
Frippiat, C. C., & Holeyman, A. E. (2008). A comparative review of upscaling methods for solute transport in heterogeneous porous media. *Journal of Hydrology*, *362*(1–2), 150–176. https://doi.org/10.1016/j.jhydrol.2008.08.015

Gardiner, C. W. (1986). Handbook of stochastic methods for physics, chemistry and the natural sciences. *Applied Optics*, *25*, 3145.
Gómez-Hernández, J. J., & Wen, X.-H. (1998). To be or not to be multi-Gaussian? A reflection on stochastic hydrogeology. *Advances in Water Resources*, *21*(1), 47–61. https://doi.org/10.1016/s0309-1708(96)00031-0
Gotovac, H., Cvetkovic, V., & Andricevic, R. (2009). Flow and travel time statistics in highly heterogeneous porous media. *Water Resources Research*, *45*(7). https://doi.org/10.1029/2008wr007168
Haggerty, R., & Gorelick, S. M. (1995). Multiple-rate mass transfer for modeling diffusion and surface reactions in media with pore-scale heterogeneity. *Water Resources Research*, *31*(10), 2383–2400. https://doi.org/10.1029/95wr10583
Hakoun, V., Comolli, A., & Dentz, M. (2019). Upscaling and prediction of Lagrangian velocity dynamics in heterogeneous porous media. *Water Resources Research*, *55*(5), 3976–3996. https://doi.org/10.1029/2018wr023810
Harvey, C., & Gorelick, S. M. (2000). Rate-limited mass transfer or macrodispersion: Which dominates plume evolution at the macrodispersion experiment (made) site? *Water Resources Research*, *36*(3), 637–650. https://doi.org/10.1029/1999WR900247
Havlin, S., & Ben-Avraham, D. (2002). Diffusion in disordered media. *Advances in Physics*, *51*(1), 187–292. https://doi.org/10.1080/00018730110116353
Hsu, K.-C. (1999). A general method for obtaining analytical expressions for the first-order velocity covariance in heterogeneous porous media. *Water Resources Research*, *35*(7), 2273–2277. https://doi.org/10.1029/1999WR900117
Hu, Y., Xu, W., Zhan, L., Ye, Z., & Chen, Y. (2020). Non-Fickian solute transport in rough-walled fractures: The effect of contact area. *Water*, *12*(7), 2049. https://doi.org/10.3390/w12072049
Hyman, J. D., Dentz, M., Hagberg, A., & Kang, P. K. (2019). Linking structural and transport properties in three-dimensional fracture networks. *Journal of Geophysical Research: Solid Earth*, *124*(2), 1185–1204. https://doi.org/10.1029/2018jb016553
Kang, P. K., Dentz, M., Le Borgne, T., & Juanes, R. (2011). Spatial Markov model of anomalous transport through random lattice networks. *Physical Review Letters*, *107*(18), 180602. https://doi.org/10.1103/physrevlett.107.180602
Kitanidis, P. K. (1988). Prediction by the method of moments of transport in a heterogeneous formation. *Journal of Hydrology*, *102*(1–4), 453–473. https://doi.org/10.1016/0022-1694(88)90111-4
Kong, B., & Chen, S. (2018). Numerical simulation of fluid flow and sensitivity analysis in rough-wall fractures. *Journal of Petroleum Science and Engineering*, *168*, 546–561. https://doi.org/10.1016/j.petrol.2018.04.070
Koponen, A., Kataja, M., & Timonen, J. (1996). Tortuous flow in porous media. *Physical Review E*, *54*(1), 406–410. https://doi.org/10.1103/physreve.54.406
Kottwitz, M. O., Popov, A. A., Baumann, T. S., & Kaus, B. J. (2020). The hydraulic efficiency of single fractures: Correcting the cubic law parameterization for self-affine surface roughness and fracture closure. *Solid Earth*, *11*(3), 947–957. https://doi.org/10.5194/se-11-947-2020
Lester, D. R., Dentz, M., Bandopadhyay, A., & Le Borgne, T. (2021). The Lagrangian kinematics of three-dimensional Darcy flow. *Journal of Fluid Mechanics*, 918.
Lester, D. R., Dentz, M., Bandopadhyay, A., & Le Borgne, T. (2022). Fluid deformation in isotropic Darcy flow. *Journal of Fluid Mechanics*, *945*, A18. https://doi.org/10.1017/jfm.2022.556
MathWorks. (2015). *Matlab version: 8.6.0 (r2015b)*. The MathWorks Inc. Retrieved from https://www.mathworks.com
Meerschaert, M. M., Benson, D. A., & Baeumer, B. (2001). Operator Lévy motion and multiscaling anomalous diffusion. *Physical Review E—Statistical Physics, Plasmas, Fluids, and Related Interdisciplinary Topics*, *63*(2), 021112. https://doi.org/10.1103/physreve.63.021112
Meyer, D. W. (2017). Relating recent random walk models with classical perturbation theory for dispersion predictions in the heterogeneous porous subsurface. *Advances in Water Resources*, *105*, 227–232. https://doi.org/10.1016/j.advwatres.2017.04.017
Meyer, D. W. (2018). A simple velocity random-walk model for macrodispersion in mildly to highly heterogeneous subsurface formations. *Advances in Water Resources*, *121*, 57–67. https://doi.org/10.1016/j.advwatres.2018.07.015
Meyer, D. W., & Tchelepi, H. A. (2010). Particle-based transport model with Markovian velocity processes for tracer dispersion in highly heterogeneous porous media. *Water Resources Research*, *46*(11). https://doi.org/10.1029/2009wr008925
Meyer, D. W., Tchelepi, H. A., & Jenny, P. (2013). A fast simulation method for uncertainty quantification of subsurface flow and transport. *Water Resources Research*, *49*(5), 2359–2379. https://doi.org/10.1002/wrcr.20240
Molz, F. J., Rajaram, H., & Lu, S. (2004). Stochastic fractal-based models of heterogeneity in subsurface hydrology: Origins, applications, limitations, and future research questions. *Reviews of Geophysics*, *42*(1). https://doi.org/10.1029/2003rg000126
Neuman, S. P., & Tartakovsky, D. M. (2009). Perspective on theories of non-Fickian transport in heterogeneous media. *Advances in Water Resources*, *32*(5), 670–680. https://doi.org/10.1016/j.advwatres.2008.08.005
Niemi, A., Bear, J., & Bensabat, J. (2017). *Geological storage of CO_2 in deep saline formations* (Vol. 29). Springer.
Painter, S. L. (1996). Evidence for non-Gaussian scaling behavior in heterogeneous sedimentary formations. *Water Resources Research*, *32*(5), 1183–1195. https://doi.org/10.1029/96wr00286
Painter, S. L., Cvetkovic, V., & Pensado, O. (2008). Time-domain random-walk algorithms for simulating radionuclide transport in fractured porous rock. *Nuclear Technology*, *163*(1), 129–136. https://doi.org/10.13182/nt08-a3976
Pollock, D. (1988). Semianalytical computation of path lines for finite-difference models. *Ground Water*, *26*(6), 743–750. https://doi.org/10.1111/j.1745-6584.1988.tb00425.x
Riva, M., Neuman, S. P., & Guadagnini, A. (2015). New scaling model for variables and increments with heavy-tailed distributions. *Water Resources Research*, *51*(6), 4623–4634. https://doi.org/10.1002/2015wr016998
Rubin, Y. (2003). *Applied stochastic hydrogeology*. Oxford University Press.
Salandin, P., & Fiorotto, V. (1998). Solute transport in highly heterogeneous aquifers. *Water Resources Research*, *34*(5), 949–961. https://doi.org/10.1029/98WR00219
Silliman, S. E., & Simpson, E. S. (1987). Laboratory evidence of the scale effect in dispersion of solutes in porous media. *Water Resources Research*, *23*(8), 1667–1673. https://doi.org/10.1029/wr023i008p01667
Song, C., Koren, T., Wang, P., & Barabási, A.-L. (2010). Modelling the scaling properties of human mobility. *Nature Physics*, *6*(10), 818–823. https://doi.org/10.1038/nphys1760
Sperl, M. (2005). Nearly logarithmic decay in the colloidal hard-sphere system. *Physical Review E—Statistical Physics, Plasmas, Fluids, and Related Interdisciplinary Topics*, *71*(6), 060401. https://doi.org/10.1103/physreve.71.060401
Wang, W., & Barkai, E. (2020). Fractional advection-diffusion-asymmetry equation. *Physical Review Letters*, *125*(24), 240606. https://doi.org/10.1103/PhysRevLett.125.240606
Wang, Z., Xu, C., Dowd, P., Xiong, F., & Wang, H. (2020). A nonlinear version of the Reynolds equation for flow in rock fractures with complex void geometries. *Water Resources Research*, *56*(2), e2019WR026149. https://doi.org/10.1029/2019wr026149
Younes, A., Ackerer, P., & Delay, F. (2010). Mixed finite elements for solving 2-D diffusion-type equations. *Reviews of Geophysics*, *48*(1). https://doi.org/10.1029/2008rg000277

Zhang, D., & Lu, Z. (2004). An efficient, high-order perturbation approach for flow in random porous media via Karhunen–Loève and polynomial expansions. *Journal of Computational Physics*, *194*(2), 773–794. https://doi.org/10.1016/j.jcp.2003.09.015

Zhang, Y., & Benson, D. A. (2013). Lagrangian simulation of multidimensional anomalous transport at the made site. *Geophysical Research Letters*, *35*(7). https://doi.org/10.1029/2008gl033222

Zhang, Y., Benson, D. A., & Reeves, D. M. (2009). Time and space nonlocalities underlying fractional-derivative models: Distinction and literature review of field applications. *Advances in Water Resources*, *32*(4), 561–581. https://doi.org/10.1016/j.advwatres.2009.01.008

Zimmerman, R. W., & Bodvarsson, G. S. (1996). Hydraulic conductivity of rock fractures. *Transport in Porous Media*, *23*(1), 1–30. https://doi.org/10.1007/bf00145263